Supplementary Material

The following supplementary material is available for this article:

Fig. S1. Age distributions of cases and controls in this study. The case appears to have two peaks, before and after around 40 years of age.

A Monte Carlo simulation experiment to compare family wise error rate for the multiple testing correction by six single nucleotide polymorphisms (SNPs) (six hypotheses examined for the joint analysis) and that by 50 SNPs (initial candidate SNPs screened in the first screening). As the framework of simulation, we set the following conditions:

Condition 1.
The total number of SNPs to be examined is set as $m = 50$ and the number of 'true' disease-associated SNPs (positive SNPs) among the 50 SNPs as $N_p = 3$ or 5.

Condition 2.
The population allelic odds ratio for the disease-associated N_p SNPs is $\psi = 1.3$, 1.5 or 1.7, while the population odds ratio for the remaining m-N_p SNPs unrelated to the disease is 1.0.

Condition 3.
In the first stage, sample size is set as 240 cases and 685 control subjects. The second stage sample size is 304 cases and 834 control subjects. In a joint analysis, sample size is set as 544 cases and 989 control subjects.

Condition 4.
The proportion of allele A in the control population is a random variable uniformly distributed in unit interval (0.05, 0.95).

Condition 5.
The criteria to evaluate the performance of each method are two indicators, sensitivity and specificity in the joint analysis.

Condition 6.
The Monte-Carlo simulation to calculate sensitivity and specificity is repeated 10 000 times, and the mean values of indicators are calculated.

Table S1 shows a summary result of the simulation experiment, which suggests that our study was designed to contain the overall false-positive (type I error) rate (1-specificity) to 5% or 8% at the power of 90%, if there are five or three true SNPs, respectively, included in our starting 50 candidate SNPs. On the other hand, the false-positive rates for the multiple testing correction by the 50 SNPs with OR = 1.5 or 1.7 are less than 1%.

Table S1. Simulation results for each multiple testing correction method

Table S2. Statistics of subgroup analysis by recessive and dominant models on all the six single nucleotide polymorphisms (SNPs) analyzed in the second stage of genotyping

This material is available as part of the online article from:
http://www.blackwell-synergy.com/doi/abs/10.1111/j.1349-7006.2008.00692.x
<http://www.blackwell-synergy.com/doi/abs/10.1111/j.1349-7006.2008.00692.x>
(This link will take you to the article abstract).

Please note: Blackwell Publishing are not responsible for the content or functionality of any supplementary materials supplied by the authors. Any queries (other than missing material) should be directed to the corresponding author for the article.

Pfetin as a Prognostic Biomarker of Gastrointestinal Stromal Tumors Revealed by Proteomics

Yoshiyuki Suehara,[1,7,8] Tadashi Kondo,[1] Kunihiko Seki,[4] Tatsuhiro Shibata,[2] Kiyonaga Fujii,[1] Masahiro Gotoh,[3] Tadashi Hasegawa,[4] Yasuhiro Shimada,[5] Mitsuru Sasako,[6] Tadakazu Shimoda,[4] Hisashi Kurosawa,[8] Yasuo Beppu,[7] Akira Kawai,[7] and Setsuo Hirohashi[1]

Abstract

Purpose: We aimed to develop prognostic biomarkers for gastrointestinal stromal tumors (GIST) using a proteomic approach.

Experimental Design: We examined the proteomic profile of GISTs using two-dimensional difference gel electrophoresis. The prognostic performance of biomarker candidates was examined using a large-scale sample set and specific antibodies.

Results: We identified 43 protein spots whose intensity was statistically different between GISTs with good and poor prognosis. Mass spectrometric protein identification showed that the 43 spots corresponded to 25 distinct gene products. Eight of the 43 spots derived from pfetin, a potassium channel protein, and four of the eight pfetin spots had a high discriminative power between the two groups. Western blotting and real-time PCR showed that pfetin expression and tumor metastasis were inversely related. The prognostic performance of pfetin was also examined by immunohistochemistry on 210 GIST cases. The 5-year metastasis-free survival rate was 93.9% and 36.2% for patients with pfetin-positive and pfetin-negative tumors, respectively ($P < 0.0001$). Univariate and multivariate analyses revealed that pfetin expression was a powerful prognostic factor among the clinicopathologic variables examined, including risk classification and c-kit– or platelet-derived growth factor receptor A mutation status.

Conclusions: These results establish pfetin as a powerful prognostic marker for GISTs and may provide novel therapeutic strategies to prevent metastasis of GIST.

Gastrointestinal stromal tumors (GIST) are the most common primary mesenchymal tumors of the digestive tract, with a prevalence of 15 to 20 per 1,000,000 (1, 2). The clinical course of GISTs spans a wide spectrum from a curable disorder to a highly malignant disease that leads to metastasis and death. Thus, the molecular background of GISTs has been extensively studied to predict the behavior of individual tumors. GISTs are characterized by the presence of mutations and overexpression of c-kit and, clinically, by their response to treatment with imatinib (3–7). Tumor location and certain molecular aberrations, including c-kit, platelet-derived growth factor (PDGFR), and p16 alterations, have been found to correlate with patient prognosis and response to treatment with imatinib (8–12). However, none of these variables has been proven to be clinically useful in improving patient outcomes yet. GISTs arise from the intestinal cells of Cajal, which are the mesenchymal pacemaker cells of the guts (13), their biological characteristics, however, remain largely obscure.

Recent comprehensive studies offered a global view of molecular aberrations associated with the malignant spectrum of GISTs. Genomic studies using fluorescence *in situ* hybridization and array-based comparative genomic hybridization identified chromosomal regions frequently amplified and target genes within these regions, the copy number status of which correlated with tumor behavior (14, 15). Global mRNA expression studies using DNA microarrays identified the genes that are involved in the signaling pathways specific to kit or PDGFR and aberrantly regulated in GISTs (16), the genes associated with histologic features denoting malignancy (17), and the genes differentially expressed based on the KIT genotype and GIST anatomic site (18). These comprehensive studies will further increase our understanding of the biology of GIST and lead to the

Authors' Affiliations: [1]Proteome Bioinformatics Project, [2]Cancer Genomics Project, and [3]Pathology Division, National Cancer Center Research Institute; [4]Clinical Laboratory Division, [5]Gastrointestinal Oncology Division, [6]Gastric Surgery Division, and [7]Orthopedic Surgery Division, National Cancer Center Hospital; and [8]Department of Orthopedic Surgery, Juntendo University School of Medicine, Tokyo, Japan

Received 6/15/07; revised 12/25/07; accepted 1/9/08.

Grant support: Ministry of Health, Labor, and Welfare and by the Program for Promotion of Fundamental Studies in Health Sciences of the National Institute of Biomedical Innovation of Japan (patent no. 2006-286087).

The costs of publication of this article were defrayed in part by the payment of page charges. This article must therefore be hereby marked *advertisement* in accordance with 18 U.S.C. Section 1734 solely to indicate this fact.

Note: Supplementary data for this article are available at Clinical Cancer Research Online (http://clincancerres.aacrjournals.org/).

Current address for T. Hasegawa: Department of Clinical Pathology, Sapporo Medical University School of Medicine.

Requests for reprints: Tadashi Kondo, Proteome Bioinformatics Project, National Cancer Center Research Institute, 5-1-1 Tsukiji, Chuo-ku, Tokyo 104-0045, Japan. Phone: 81-3-3542-2511, ext. 3004; Fax: 81-3-357-5298; E-mail: takondo@gan2.res.ncc.go.jp.

doi:10.1158/1078-0432.CCR-07-1478

Table 1. Clinicopathologic features of the training set samples (17 cases)

Sample No	Age	Gender	Site	Histologic types	Size (cm)	Risk classification*
1	68	M	Stomach	Spindle	19	High
2	56	M	Stomach	Spindle	38	High
3	58	M	Stomach	Spindle	13	High
4	50	F	Rectum	Spindle	4	High
5	51	M	Stomach	Mixed (spindle main)	12	High
6	34	M	Small intestine	Spindle	18	High
7	68	M	Small intestine	Mixed (spindle main)	7	High
8	72	F	Stomach	Spindle	25	High
9	64	F	Stomach	Spindle	3.5	Low
10	64	F	Stomach	Spindle	4	Low
11	54	M	Stomach	Spindle	10	Intermediate
12	68	M	Small intestine	Spindle	3.7	Low
13	77	M	Small intestine	Spindle	4	Low
14	40	F	Stomach	Spindle	10	Intermediate
15	52	M	Stomach	Spindle	7	Intermediate
16	76	M	Small intestine	Spindle	7	Intermediate
17	81	M	Stomach	Spindle	5.5	Intermediate

NOTE: PDGFR mutations: All samples lacked of PDGFR mutations. Detail data: Supplementary Table S1.
Abbreviations: NED, no evidence of disease; AWD: alive with disease; DOD, dead of disease.
*Prognostic classification based on tumor size and MIB-1 grade (Hasegawa, T. et al. Hum Pathol. 2002, 33:669-676).

development of practical tumor markers to support individualized therapy (8). Emerging technologies that examine the overall features of the expressed proteins, namely the proteome, have identified many candidate proteins associated with early diagnosis (19), differential diagnosis (20), prognosis (21), and response to chemotherapy (22) in various diseases. Many lines of evidence have indicated that DNA copy number and mRNA expression levels do not necessarily correspond to the protein contents, and that posttranslational modifications cannot be predicted by DNA sequences (23, 24), suggesting that proteomic studies offer unique data that cannot be obtained by other approaches. The proteomic profile of GISTs has not been established yet, and a proteomic study using a large-scale clinical sample set would complement the genome and transcriptome studies.

In this report, we did a comprehensive quantitative expression study on the intact proteins of GIST clinical samples using two-dimensional difference gel electrophoresis and mass spectrometry. Proteomic studies on peptides have been used to develop tumor markers, but intact proteins have not been considered for this purpose, with a few exceptions. Two-dimensional difference gel electrophoresis, as the most advanced form of two-dimensional gel electrophoresis, has the great advantage of being able to be used to study intact proteins. We found that the expression levels of 43 proteins, including eight variants of pfetin (predominantly fetal-expressed tetramerization domain; potassium channel tetramerisation domain containing protein 12), which was originally reported as a protein highly expressed in fetal cochlea and brain (25), correlated with prognosis. We verified the prognostic value of pfetin expression on 210 GIST cases using immunohistochemistry. Our findings indicate that the use of pfetin expression as a prognostic indicator may facilitate tailored medical care for GIST patients.

Materials and Methods

Patients and clinical information. We examined the tumor tissues of 212 GIST patients who underwent surgery at the National Cancer Center Hospital consecutively from October 1977 to December 2005. All patients underwent resection with curative intent and were not treated with adjuvant chemotherapy, including treatment with imatinib, until distant metastasis was diagnosed. Histologic features of the tissues were reviewed by three board-certified pathologists (K.S., T.S., and T.H.). Diagnosis was based on the WHO classification system for soft-tissue tumors (26), including the examination of tumor size, presence of necrosis, differentiation, mitotic rate, MIB-1 index, presence of epithelioid cells, and CD34 and CD117 expression. Using this large, well-characterized single hospital–based sample set, we were able to identify proteomic features that differ significantly when examined in relation to certain clinicopathologic variables. This project was approved by the institutional review board of the National Cancer Center.

Previous reports indicated that GIST patients that were histologically classified as of being at low or intermediate risk did not develop metastases within 2 y postsurgery, whereas GIST patients histologically classified as of being at high risk developed metastases within 1 y postsurgery (27). For proteomic analysis, we grouped the GIST samples into two groups. GISTs that had metastases at diagnosis or developed metastases within 1 y postsurgery and were categorized in the high-risk group based on their histologic features were defined as poor-prognosis GISTs (P-GIST; Table 1, samples 1-8). GISTs that did not have metastases within 2 y postsurgery and were grouped in the low- or intermediate-risk group based on the histologic features were defined as good-prognosis GISTs (G-GIST; Table 1, samples 9-17). The samples listed in Supplementary Table S1 were excluded from this classification; samples 18, 19, 24, and 25 were excluded because RNA data were not available for the validation study and the other samples because they did not meet the criteria for classification either as P-GISTs or G-GISTs.

For the immunohistochemical study, we selected 210 patients who did not have distant metastases at the time of surgery.

Protein expression profiling. Frozen samples were crushed to powder with a CryoPress (Microtech Nichion) under cooling with liquid nitrogen. The frozen powder was then treated with urea lysis buffer

Table 1. Clinicopathologic features of the training set samples (17 cases) (Cont'd)

Type of KIT mutation	Metastatic site (first development)	Metastasis time after diagnosis (mo)	Follow-up time after diagnosis (mo)	Follow-up status
Wild-type	Peritoneal metastasis	8	16	DOD
EX11 deletion	Peritoneal metastasis	7	9	DOD
EX11 deletion	Peritoneal metastasis	6	11	DOD
EX11 deletion	Peritoneal metastasis	11	60	AWD
EX11 deletion	Peritoneal metastasis	5	69	AWD
EX11 deletion	Liver metastasis	At diagnosis	31	AWD
EX9 insertion	Peritoneal metastasis	At diagnosis	9	AWD
EX11 559 V-D	Peritoneal metastasis	5	8	AWD
Wild-type	—	—	68	NED
Wild-type	—	—	81	NED
EX11 560 V-G	—	—	77	NED
EX9 insertion	—	—	50	NED
Wild-type	—	—	69	NED
EX11 559 V-D	—	—	88	NED
EX11 576 L-P	—	—	62	NED
EX11 deletion	—	—	48	NED
EX11 559 V-D	—	—	43	NED

(6 mol/L urea, 2 mol/L thiourea, 3% CHAPS, and 1% Triton X-100). After centrifugation at 15,000 rpm for 30 min, the supernatant was used as the source of cellular proteins for protein expression studies.

Two-dimensional difference gel electrophoresis was done as described previously (20, 28, 29). In brief, the internal control sample was prepared by mixing a portion of all individual samples. Five micrograms of the internal control sample and of each individual sample were labeled with Cy3 and Cy5, respectively (CyDye DIGE Fluor saturation dye; GE Healthcare Biosciences) according to the manufacturer's instructions. The differently labeled protein samples were mixed and separated by two-dimensional gel electrophoresis, which was achieved using IPG DryStrip gels for the first dimension separation (length, 24 cm; isoelectric point range, between 4 and 7; GE Healthcare Biosciences) and SDS-PAGE for the second dimension separation (EttanDalt II; GE Healthcare Biosciences). The gels were scanned using laser scanners (Tyhoon Trio; GE Healthcare Biosciences) at appropriate wavelengths. For all spots, the intensity of the Cy5 image was normalized by that of the Cy3 image in the identical gel so that gel-to-gel differences were compensated, using the DeCyder image software (GE Healthcare Biosciences). System reproducibility was verified by comparing the protein profiles obtained from three independent separations of the identical sample (sample 22; Supplementary Table S1). Scatter plot analysis revealed that the standardized intensity of >96% of the spots ranged within a 2.0-fold difference (Supplementary Fig. S1). Representative two-dimensional images with the numbers of the identified spots are shown in Fig. 1A and Supplementary Fig. S3.

Data analysis. We identified protein spots whose intensity was statistically (Wilcoxon test, $P < 0.001$) different between the groups examined. Hierarchical clustering, principal component analysis, correlation matrix study, and spot ranking were done using the Expressionist software (Genedata).

Protein identification by mass spectrometry. Proteins corresponding to the spots of interest were identified by mass spectrometry according to our previous report (20, 30). Cy5-labeled proteins separated by 2D-PAGE were recovered in gel plugs and digested with modified trypsin (Promega). The trypsin digests were subjected to liquid chromatography coupled with tandem mass spectrometry equipped with a nanoelectrospray ion source (Paradigm MS4 dual solvent delivery system; Michrom BioResources, Inc.) for microflow high performance liquid chromatography, an HTS PAL auto sampler (CTC Analytics), and a Finnigan LTQ linear ion trap mass spectrometer (Thermo Electron Co.) equipped with a nanoelectrospray ion source (AMR, Inc.). The Mascot software (version 2.1; Matrix Science) was used to search for the mass of the peptide ion peaks against the SWISS-PROT database (Homo sapiens, 12867 sequence in Sprot_47.8 fasta file). Proteins with a Mascot score of 35 or more were used for protein identification. When multiple proteins were identified in a single spot, the proteins with the highest number of peptides were considered as those corresponding to the spot.

Western blotting and immunohistochemistry. Protein samples were separated by SDS-PAGE and subsequently blotted on a nitrocellulose membrane. The membrane was incubated with rabbit polyclonal antibody against pfetin (1:1,000 dilution) kindly provided by Dr. Morton (25), and then horseradish peroxidase-conjugated secondary antibody (1:1,000 dilution; GE Healthcare Biosciences). Pfetin was detected using an emhanced chemiluminescence system (GE Healthcare Biosciences) and LA 1000 (Fuji film).

Pfetin expression was examined immunohistochemically using paraffin-embedded tissues. In brief, 4-μm-thick tissue sections were autoclaved in 10 mmol/L citrate buffer (pH 6.0) at 121°C for 30 min and incubated with the antibody against pfetin (1:500 dilution). Immunostaining was done according to the streptavidin-biotin peroxidase method using the Strept ABC Complex/horseradish peroxidase kit (DAKO). One pathologist (K. S.) and one medical doctor (Y. S.) reviewed the sections stained with antipfetin antibody in a blinded fashion regarding clinical data (age, sex, anatomic site, and outcome). Positively stained cells were defined as those that had higher staining intensity than that of vascular endothelial cells, which served as positive controls. Cases with >20% of tumor cells stained positively with the antipfetin antibody were considered as pfetin positive, whereas cases with <20% pfetin-positive tumor cells were considered as pfetin negative. In most cases, the difference was so obvious that two reviewers had consistent results. Inconsistencies, if any, were resolved by discussion, as a usual process of pathologic diagnosis in the hospital.

Mutation study for c-kit and PDGFRA. We examined the c-kit and PDGFRA genes for the presence of mutations as previously described (31) in the 39 cases where DNA samples were available. In brief, DNA was extracted from the frozen tissues, and the exons including the frequent mutation sites for c-kit and PDGFRA were amplified by PCR. The PCR products were purified with 2% agarose gel electrophoresis, extracted with an QIAquick PCR Purification kit (Qiagen), and sequenced using an ABI Prism 3100 Genetic Analyzer (Applied Biosystems). The primer sets for c-kit were as follows: 5′-TCTAGTGCATTCAAGCACAATGG-3′ and 5′-CATGACTGATATGGTAGACAGAG-3′ for exon 9, and 5′-CCAGAGTGCTCTAATGACTGAGAC-3′ and 5′-AAAGGTGACATGGAAAGCCCCTG-3′ for exon 11.The primer set for exon 12 of the PDGFRA gene was 5′-CCTGGTCATTTATAGAAACCGAG-3′

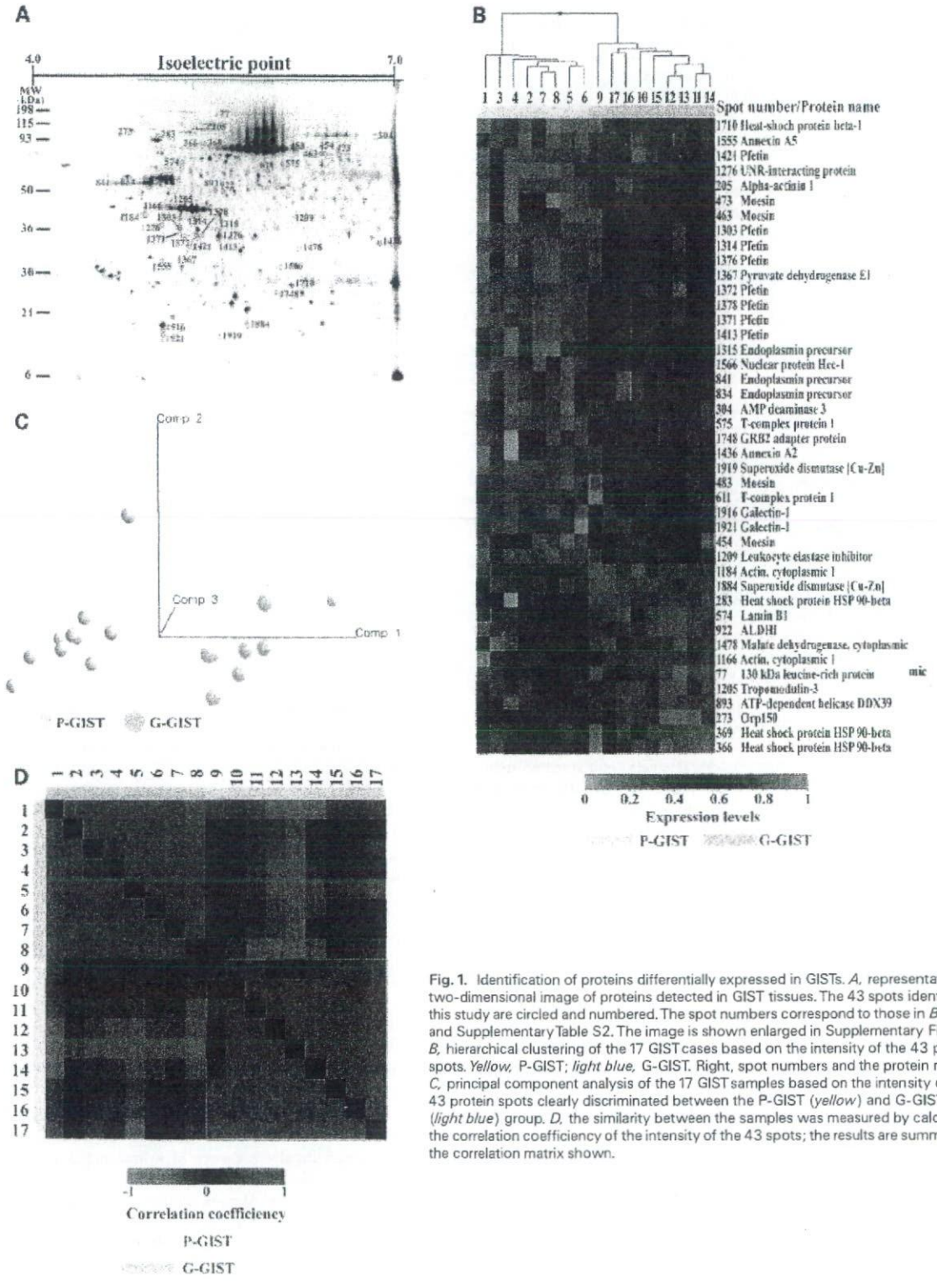

Fig. 1. Identification of proteins differentially expressed in GISTs. *A,* representative two-dimensional image of proteins detected in GIST tissues. The 43 spots identified in this study are circled and numbered. The spot numbers correspond to those in *B*, Table 2, and Supplementary Table S2. The image is shown enlarged in Supplementary Fig. S3. *B,* hierarchical clustering of the 17 GIST cases based on the intensity of the 43 protein spots. *Yellow,* P-GIST; *light blue,* G-GIST. Right, spot numbers and the protein names. *C,* principal component analysis of the 17 GIST samples based on the intensity of the 43 protein spots clearly discriminated between the P-GIST (*yellow*) and G-GIST (*light blue*) group. *D,* the similarity between the samples was measured by calculating the correlation coefficiency of the intensity of the 43 spots; the results are summarized in the correlation matrix shown.

and 5′-CTCCCATCTTGAGTCATAAGGCA-3′. PCR cycling variables were as follows: cycle at 96°C for 1 min; 50 cycles at 94°C for 30 s, 56°C for 30 s, and 68°C for 2.5 min; and finally 1 cycle at 72°C for 5 min.

Quantitative reverse transcription-PCR. We extracted mRNA and generated cDNA using the Super Script III kit (Invitrogen) in the 39 cases where mRNA samples were available. The quantitative amplification was monitored with Taq Man Gene Expression Assays

Table 2. A list of identified protein

Spots no*	Accession no†	Identified protein†	Wilcoxon test *P*	Fold difference (ratio of means)	Overall rank
1378	Q96CX2	Potassium channel tetramerisation domain containing protein 12 (Pfetin)	8.23E-05	4.862	1
1314	Q96CX2	Potassium channel tetramerisation domain containing protein 12 (Pfetin)	8.23E-05	5.805	2
1,371	Q96CX2	Potassium channel tetramerisation domain containing protein 12 (Pfetin)	8.23E-05	3.781	5
1413	Q96CX2	Potassium channel tetramerisation domain containing protein 12 (Pfetin)	1.65E-04	3.198	26
575	P17987	T-complex protein 1, α subunit	3.29E-04	1.405	28
893	O00148	ATP-dependent helicase DDX39	6.99E-04	2.321	41
1367	P11177	Pyruvate dehydrogenase estrone component β subunit	8.94E-04	3.669	24
1303	Q96CX2	Pfetin	9.87E-04	2.917	4
1919	P00441	Superoxide dismutase (Cu-Zn)	1.33E-03	2.547	12
611	P17987	T-complex protein 1, α subunit	1.56E-03	1.982	9
1184	P60709	Actin, cytoplasmic 1	1.56E-03	1.902	20
1376	Q96CX2	Pfetin	1.56E-03	2.850	38
834	P14625	Endoplasmin precursor	1.75E-03	3.487	8
483	P26038	Moesin	1.86E-03	1.558	15
369	P08238	Heat shock protein HSP 90-β	1.86E-03	1.977	16
922	P05091	Aldehyde dehydrogenase, mitochondrial precursor	2.04E-03	1.359	31
273	Q9Y4L1	150 kDa oxygen-regulated protein precursor	3.32E-03	1.384	36
1436	P07355	Annexin A2	3.32E-03	1.590	39
1,748	P62993	Growth factor receptor-bound protein 2	3.32E-03	1.545	40
205	P12814	α-actinin 1	3.70E-03	1.993	11
1710	P04792	Heat-shock protein β-1	3.70E-03	2.078	13
574	P20700	Lamin B1	3.70E-03	2.575	14
1555	P08758	Annexin A5	3.70E-03	1.438	19
454	P26038	Moesin	3.70E-03	1.441	37
1315	P14625	Endoplasmin precursor	3.73E-03	2.895	23
1276	Q9Y3F4	Serine-threonine kinase receptor-associated protein	3.85E-03	1.650	29
304	Q01432	AMP deaminase 3	4.00E-03	1.691	22
1372	Q96CX2	Pfetin	4.04E-03	2.972	30
1478	P40925	Malate dehydrogenase, cytoplasmic	4.08E-03	1.534	27
1916	P09382	Galectin-1	4.21E-03	1.917	7
1209	P30740	Leukocyte elastase inhibitor	4.33E-03	2.380	18
1884	P00441	Superoxide dismutase (Cu-Zn)	5.25E-03	3.121	3
77	P42704	130 kDa leucine-rich protein	5.51E-03	1.456	21
1166	P60709	Actin, cytoplasmic 1	5.51E-03	3.971	42
1921	P09382	Galectin-1	6.22E-03	1.912	6
1421	Q96CX2	Pfetin	6.22E-03	1.665	34
366	P08238	Heat shock protein HSP 90-β	7.02E-03	1.705	25
1566	P82979	Nuclear protein Hcc-1	7.02E-03	1.526	43
473	P26038	Moesin	7.59E-03	1.323	32
1205	Q9NYL9	Tropomodulin-3	7.90E-03	1.935	10
283	P08238	Heat shock protein HSP 90-β	7.90E-03	1.300	33
463	P26038	Moesin	7.90E-03	1.524	35
841	P14625	Endoplasmin precursor	9.45E-03	2.478	17

*Spot numbers refer to those in Fig. 1A and Supplementary Fig. S3.
†Accession numbers of protein were derived from SWISS-PROT and National Center for Biotechnology Information nonredundant databases.
‡Observed isoelectric point and molecular weight calculated according to location on the two-dimensional gel.
§Theoretical isoelectric point and molecular weight obtained from Swiss-Prot and the ExPASy database. (http://au.expasy.org).
‖Mascot score for the identified proteins based on the peptide ions score ($P < 0.05$; http://www.matrixscience.com).

using premade primers for pfetin and Human glyceraldehyde-3-phosphate dehydrogenase, and Taq Man Universal PCR Master Mix with 7500 Real-time PCR system (Applied Biosystems) according to the manufacturer's instructions.

Statistical analysis. The tumor-specific and metastasis-free survival times were calculated from the first resection of the primary tumor to death from tumor-specific causes or to first evidence of metastasis, respectively. All time-to-event end points were computed by the Kaplan-Meier method (32). Patients who died of causes unrelated to GISTs were censored at the time of death. Potential prognostic factors were identified by univariate analysis using the log-rank test. Independent prognostic factors were evaluated using a Cox's proportional hazards regression model and a stepwise selection procedure. To arrive at a parsimonious multivariate model, covariates were selected into the

Table 2. A list of identified protein (Cont'd)

pI (obs)‡	pI (cal)§	MW (obs; kDa)‡	MW (cal; kD)§	Protein score‖	Peptide matches	Sequence coverage (%)
6.4	5.5	35.1	35.7	406	8	20.0
5.4	5.5	44.0	35.7	338	7	19.7
6.2	5.5	35.7	35.7	146	2	8.3
6.5	5.5	34.5	35.7	306	8	23.4
5.1	5.8	73.3	60.3	267	6	12.4
5.5	5.5	51.8	49.1	109	2	3.7
6.4	6.2	35.1	39.2	174	3	9.7
5.2	5.5	44.7	35.7	236	5	14.5
6.6	5.7	15.3	15.8	60	1	7.8
4.9	5.8	67.9	60.3	667	11	22.5
5.9	5.3	46.3	41.7	276	4	11.2
6.5	5.5	35.1	35.7	396	11	23.7
4.7	4.8	57.2	92.5	977	18	20.5
5.2	6.1	84.0	67.7	208	4	6.9
4.4	5.0	89.4	83.1	263	5	7.3
5.6	6.6	50.0	56.4	323	5	10.1
4.7	5.2	113.7	111.3	102	2	2.4
6.9	7.6	34.5	38.5	262	5	13.3
6.0	5.9	25.5	25.2	79	2	7.4
4.4	5.3	114.1	103.1	593	12	12.9
6.1	6.0	27.5	22.8	491	15	54.1
4.2	5.1	75.1	66.3	1616	33	36.4
6.1	4.9	31.5	35.8	96	2	5.3
5.4	6.1	82.3	67.7	366	8	9.2
5.5	4.8	44.3	92.5	216	5	4.7
5.1	5.0	45.0	38.4	250	5	15.4
4.8	6.5	113.4	88.8	185	3	4.6
6.3	5.5	35.1	35.7	118	2	8.3
6.2	6.9	33.6	36.3	116	2	5.7
6.1	5.3	16.9	14.6	244	6	35.8
5.2	5.9	46.0	42.7	551	9	23.0
6.8	5.7	18.4	15.8	139	2	17.0
4.5	5.5	195.2	145.2	120	2	1.7
5.9	5.3	46.3	41.7	246	7	15.5
6.1	5.3	15.8	14.6	90	3	11.9
6.4	5.5	34.5	35.7	336	13	23.4
4.4	5.0	89.4	83.1	420	8	13.8
6.1	6.1	30.6	23.5	196	2	13.9
5.6	6.1	80.5	67.7	775	15	18.8
5.2	5.1	46.0	39.6	168	3	9.1
4.1	5.0	113.1	83.1	907	17	22.1
5.4	6.1	82.3	67.7	356	7	9.7
4.7	4.8	57.2	92.5	159	3	4.0

model only if they contributed significantly to the fit of the model based on the χ^2 test value. *P* value differences of <0.05 were considered to be significant. Statistical analyses were done using the SPSS statistical package (SPSS).

Results

We compared the protein expression profiles between nine G-GISTs and eight P-GISTs using two-dimensional difference gel electrophoresis. We selected 1,513 protein spots that appeared in at least 75% of the images of the Cy3-labeled internal control sample to decrease irrelevant expression data. The G- and P-GIST samples were not classified into their respective groups based on the overall protein expression features of the samples (Supplementary Fig. S2). However, we found that 43 protein spots had significantly different intensity between the two groups ($P < 0.01$). The localization of the 43 spots on the two-dimensional image is shown in Fig. 1A (enlarged image in Supplementary Fig. S3). Hierarchical clustering and principal component analysis accurately classified the 17 GIST samples into either the G- or the P-GIST group based on the intensity of the 43 selected spots (Fig. 1B and C). The profiles of the 43 spots were similar between samples of the same group and different between

the two groups (Fig. 1D). Mass spectrometric protein identification revealed that the 43 protein spots corresponded to 25 distinct gene products (Fig. 1B; Table 2; Supplementary Table S2).

We aimed to prioritize the protein spots according to their discriminative power for the two groups. We created a classifier based on a support vector machine algorithm that used the intensity of the 43 spots and ranked the 43 spots according to their contribution to the classification using support vector machine weight algorithm (Table 2). We found that 4 of the 8 identified pfetin spots were ranked within the top 10 protein spots whose intensity was different between the groups (Table 2), and that pfetin spots appeared 8 times in the list of the 43 protein spots (Fig. 1B; Table 2).

Pfetin is highly expressed in fetal cochlea and brain (25), consistent with the fact that the origin of GIST is Cajal cells, neuronal cells in the gut. Thus, we further validated the relationship of the expression of pfetin with the malignant potential of GISTs. SDS-PAGE/Western blotting showed that the expression of pfetin was lower in the P-GIST compared with the G-GIST group (Fig. 2A). Two bands on SDS-PAGE/Western blotting corresponded to the location of protein spots for pfetin variants on the two-dimensional image (Fig. 1A; Supplementary Fig. S3). These results were further validated in an additional four GIST samples that were not included in the initial proteome study (Supplementary Fig. S4A). Pfetin expression was not observed in the 6 liver metastases examined or in primary high-risk GISTs that developed metastases between 13 and 30 months postsurgery (Supplementary Fig. S4B; Supplementary Table S1).

We used immunohistochemistry to evaluate pfetin expression *in situ*. Positive cells were diffusely stained with antipfetin antibody in membrane and cytoplasm. All nine G-GISTs expressed pfetin, whereas none of the eight P-GISTs did (Fig. 2B). Pfetin expression was not observed in neighboring host cells or in the intestinal cells of Cajal (Supplementary Fig. S5).

Real-time RT-PCR revealed pfetin mRNA levels were higher in G-GISTs than in P-GISTs (Fig. 2C). However, the difference between the P- and G- GIST group was less obvious at the mRNA than at the protein level, suggesting that pfetin expression is partially regulated at the mRNA level, and that

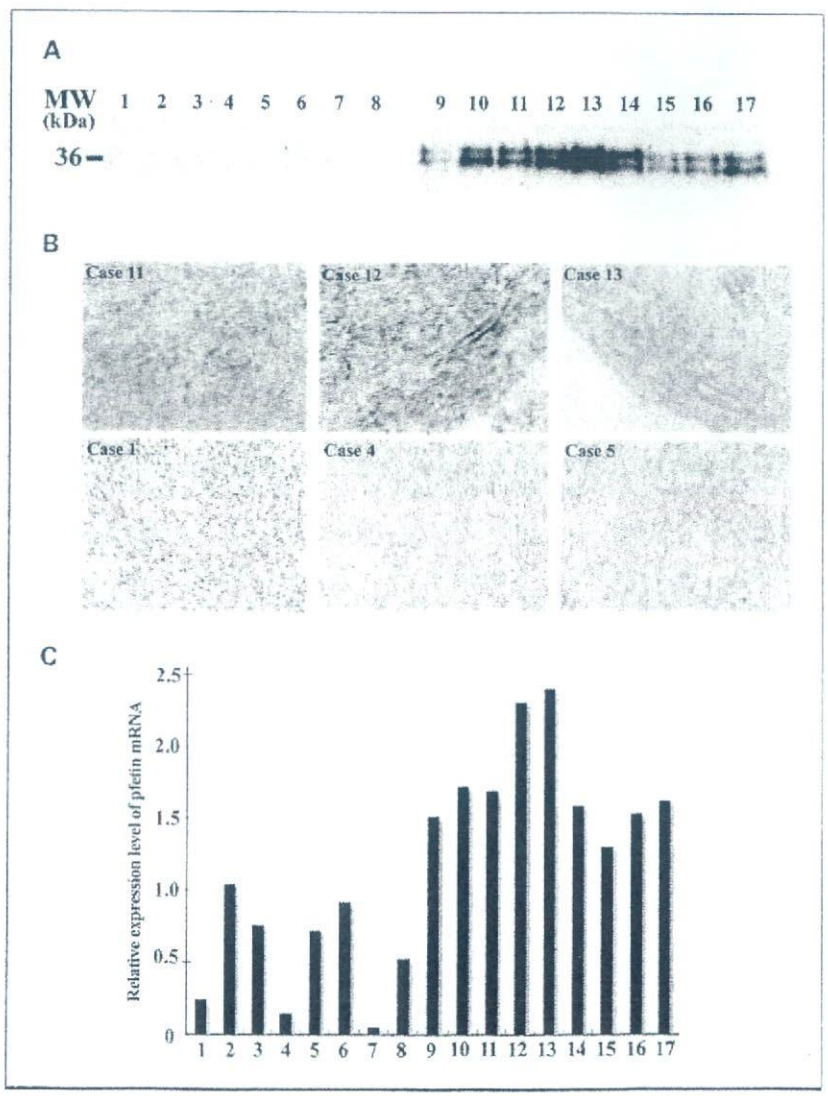

Fig. 2. Validation of the differential expression of pfetin. G-GISTs expressed pfetin at significantly higher levels than P-GISTs. *A*, Western blotting. Case numbers correspond to those in Fig. 1. *B*, immunohistochemistry; pfetin is overexpressed in G-GISTs (*top*), whereas it is not expressed in P-GISTs (*bottom*). *C*, the pfetin mRNA expression levels detected in the 17 GIST samples examined. P-GIST, 1:8; G-GIST, 9:17.

posttranscriptional regulation may also play an important role in pfetin expression.

As pfetin expression has been reported to correlate with c-kit mutation status (33), we examined 39 primary GISTs for the presence of c-kit and PDGFRA gene mutations and monitored their pfetin expression levels by Western blotting (Supplementary Tables S1 and S3). Overexpression of pfetin was observed in 12 of 29 c-kit mutation positive cases and in 6 of 10 negative cases ($P = 0.389$; Supplementary Table S3). PDGFRA mutations were not detected in the series. We observed no significant correlation between pfetin expression and c-kit or PDGFR mutation status.

The immunohistochemical study of 210 GISTs revealed a strong correlation between pfetin expression and a number of clinicopathologic variables including the tumor size, mitotic index, MIB-1 index, degree of differentiation, and risk classification ($P < 0.0001$; Table 3). Moreover, distant metastasis was observed in a significantly higher proportion of patients with pfetin-negative tumors compared with those with pfetin-positive tumors (24 of 39 versus 12 of 171 cases; $P < 0.0001$), with a median follow-up period of 73 months. The 5-year metastasis-free survival rate was significantly higher in the pfetin-positive than in the negative group overall (93.9% versus 36.2%; $P < 0.0001$; Fig. 3A; Table 3) as well as within each risk group (Fig. 3B-D). Multivariate analysis revealed that pfetin expression was a powerful predictor of disease-specific survival (Table 3). Note that high-risk cases were divided into two groups, the pfetin-positive and the pfetin-negative group, the latter having a worse prognosis. Furthermore, tumor-specific survival was statistically significantly longer in the pfetin-positive compared with the pfetin-negative group ($P < 0.0001$; Table 3; Supplementary Fig. S6). These data

Table 3. Univariate and multivariate analysis of prognostic factor and the relationship between clinicopathologic variables and pfetin expression

Variable	Number of cases	Metastasis-free survival		Tumor-specific survival		Multivariate analysis of metastasis free survival by Cox regression			Pfetin positive (no. cases)	Pfetin negative (no. cases)	Correlation (pfetin) χ^2 (P)
		5 y (%)	Log-rank (P)	5-y (%)	Log-rank (P)	P	Relative risk	95% CI			
Age			0.3290		0.8350						0.5220
<60	112	85.8 ± 3.7		91.8 ± 3.0					93	19	
60<	98	80.7 ± 4.2		95.6 ± 2.2					78	20	
Sex			0.4420		0.0393						0.8909
F	99	86.5 ± 3.7		96.1 ± 2.2					81	18	
M	111	80.4 ± 4.2		91.6 ± 2.8					90	21	
Site			0.0001		0.1655						0.4776
Stomach	170	87.8 ± 2.7		93.9 ± 2.0					140	30	
Nonstomach	40	60.7 ± 9.2		92.2 ± 5.3		0.0270	2.21	1.09-4.49	31	9	
Histology			0.1003		0.2068						0.5153
Spindle	189	85.4 ± 2.8		93.6 ± 2.0					155	34	
Epithelioid	21	67.7 ± 10.9		95.2 ± 4.6					16	5	
Size			<0.0001		<0.0001						<0.0001
<5 cm	128	92.4 ± 2.6		98.1 ± 1.3					112	16	
5-10 cm	63	76.6 ± 0.4		93.7 ± 3.5					51	12	
15 cm<	19	45.0 ± 11.9		60.5 ± 13.0		0.0070	2.05	1.22-3.44	8	11	
Necrosis			<0.0001		0.0034						0.0070
+	19	43.0 ± 12.7		76.9 ± 11.7					10	30	
-	191	86.9 ± 2.7		95.1 ± 1.7					161	9	
Miosis			<0.0001		<0.0001						<0.0001
<5/50HPF*	148	95.5 ± 2.0		98.2 ± 1.3					136	12	
5-10/50HPF	33	80.4 ± 7.2		96.8 ± 3.2					26	7	
5/50HPF<	29	29.9 ± 9.0		68.2 ± 9.4					9	20	
MIB-1			<0.0001		<0.0001						<0.0001
<9%	164	96.0 ± 1.8		98.4 ± 1.1					152	12	
10-29%	19	51.4 ± 12.6		85.6 ± 9.7					11	8	
<30%	27	32.5 ± 9.6		70.8 ± 9.4					8	19	
Differentiation			<0.0001		<0.0001						<0.0001
Score 1	161	95.9 ± 1.8		98.4 ± 1.1					149	12	
Score 2	49	43.5 ± 7.7		78.1 ± 6.6		<0.0001	10.40	3.68-29.45	22	27	
Risk classification			<0.0001		<0.0001						<0.0001
Low	110	97.7 ± 1.6		98.9 ± 1.1					100	10	
Intermediate	46	90.6 ± 5.2		97.0 ± 3.0					44	2	
High	54	48.5 ± 7.4		80.6 ± 6.0					27	27	
Pfetin			<0.0001		<0.0001						
Positive	171	93.9 ± 2.0		97.2 ± 1.4							
Negative	39	36.2 ± 8.7		76.5 ± 7.9		0.0020	3.75	1.60-8.81			

Abbreviation: 95% CI, 95% confidence interval.
*HPF, high-power field.

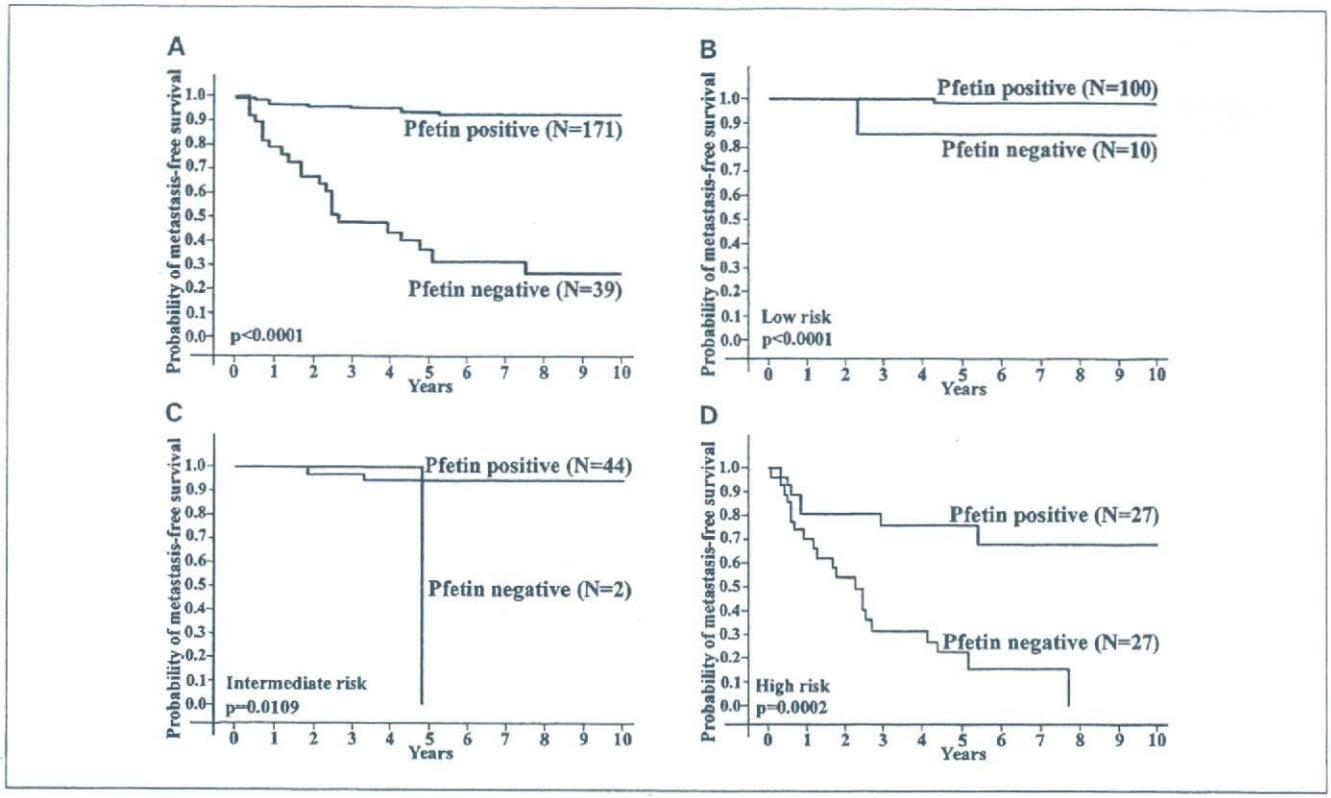

Fig. 3. Pfetin expression in the primary tumor samples was predictive of the metastasis-free survival period. Statistically significant differences in the metastasis-free survival period were observed between the pfetin-positive and pfetin-negative groups ($P < 0.0001$) both for the M0 GIST patients overall (*A*) and within each risk group of patients (*B-D*).

clearly indicate that prognosis relying solely on the established risk classification system is not sufficiently accurate to determine the post-operative therapeutic strategy for GIST patients, and the use of pfetin expression may further refine the prognostic criteria so as to identify patients who may benefit from additional therapy.

Discussion

Employing proteomics tools, we identified 43 protein variants corresponding to 25 distinct gene products that distinguished GIST patients according to their clinical outcome. The discriminating power of this set of proteins may be developed for use in a clinical setting. However, albeit useful to describe complex clinical variables, cutting-edge proteomic technologies cannot be transferred easily to a hospital setting, considering the high installation costs and labor intensity, the low throughput, and the required operational skills. A smaller number of proteins, measurable by simpler techniques, may be preferable for use in practice. With this notion, we showed that pfetin expression can be examined by SDS-PAGE/Western blotting, immunohistochemistry, and quantitative RT-PCR. Moreover, using a large-scale sample set, we showed that the expression levels of pfetin, as evaluated by immunohistochemistry, are predictive of patient outcome. Therefore, evaluation of pfetin expression can be applied in a clinical setting using the existing examination protocol and may allow the identification of a high-risk patient group that may benefit from adjuvant therapy, such as treatment with imatinib, while it may also help spare low-risk patients unnecessary treatment. As mass spectrometric global surveys for phosphorylated proteins identified pfetin as a phosphorylated protein (34, 35), the multiple protein spots of pfetin may correspond to the different phosphorylation variants.

Recently, Kang et al. (33) did a proteomic study on 12 GIST samples using two-dimensional gel electrophoresis and reported that pfetin overexpression (C13orf2 in their report) correlated with histologic grading and the presence of c-kit mutations. In contrast, our results indicated that pfetin expression is inversely correlated with histologic grading (Figs. 1 and 2), and that pfetin expression levels are not associated with c-kit mutation status (Supplementary Tables S1 and S3). Moreover, the proteins reported to correlate with histologic malignancy by Kang et al. (33), including Annexin V, HMGB1, glutamate dehydrogenase 1, and fibrinogen β chain RoXaN (33), were not identified as such in our study, whereas 24 gene products identified in this study were not listed in their report (33). As these discrepancies may be due to differences in patient populations and proteomic modalities used, an international project to integrate all reported proteomic data in a common proteomic platform is needed to elucidate the molecular background of GISTs.

Although pfetin is known to contain a voltage-gated potassium (K^+) channel tetramerization domain (25), its function in the process of cancer development and progression

is unknown. Although GISTs originate from Cajal cells, immunohistochemistry revealed that pfetin was absent in Gajal cells (Supplementary Fig. S5). Proteomic analysis of pfetin-associated proteins may provide clues to understanding the role of pfetin in GIST development and progression.

Our study has the limitation of not detecting proteins expressed in low levels. We did not observe overexpression of the kit (36–41) or PDGFRA gene products, or loss of CD44 (42) or p16 (11, 12). In addition, we did not detect CD34 (18) or connexin 43 (43) expression, reported to be commonly up-regulated in stomach and small intestinal GISTs, respectively. Aberrant regulation of these gene products was initially detected at the mRNA level and was later confirmed at the protein level using specific antibodies. Presently, any global approach to protein expression cannot uncover the whole proteome in a quantitative and reproducible way. The continuing efforts to improve the sensitivity of proteomic modalities have enabled the uncovering of several thousands of proteins with posttranslational modifications (24, 44, 45). We believe that such efforts will overcome some of the inherent limitations of proteomics and lead to a more detailed understanding of the disease mechanisms and to novel therapeutic strategies in the near future.

In conclusion, we identified a possible correlation of 43 protein variants corresponding to 25 distinct gene products with variables of clinical interest in GIST and validated pfetin expression using a specific antibody. From this study, pfetin expression is predictive of metastasis and survival of patients with GISTs and, as such, may be used in clinical practice to improve existing therapeutic strategies. Assessment of the prognostic power of the combined use of pfetin and the other 24 proteins as well as more extensive validation of pfetin using additional samples are now under way in our laboratory.

Acknowledgments

We thank Kiyoaki Nomoto, Chizu Kina, and Sachiko Miura for their excellent technical support in the immunohistochemical study, and Kano Nishiyama and Yukiko Fujie in electrophoresis.

References

1. Joensuu H, Kindblom LG. Gastrointestinal stromal tumors-a review. Acta Orthop Scand Suppl 2004;75:62–71.
2. Miettinen M, El-Rifai W, HL Sobin L, Lasota J. Evaluation of malignancy and prognosis of gastrointestinal stromal tumors: a review. Hum Pathol 2002;33:478–83.
3. Corless CL, Fletcher JA, Heinrich MC. Biology of gastrointestinal stromal tumors. J Clin Oncol 2004;22:3813–25.
4. Heinrich MC, Rubin BP, Longley BJ, Fletcher JA. Biology and genetic aspects of gastrointestinal stromal tumors: KIT activation and cytogenetic alterations. Hum Pathol 2002;33:484–95.
5. Miettinen M, Majidi M, Lasota J. Pathology and diagnostic criteria of gastrointestinal stromal tumors (GISTs): a review. Eur J Cancer 2002;38 Suppl 5:S39–51.
6. Demetri GD, von Mehren M, Blanke CD, et al. Efficacy and safety of imatinib mesylate in advanced gastrointestinal stromal tumors. N Engl J Med 2002;347:472–80.
7. van Oosterom AT, Judson I, Verweij J, et al. Safety and efficacy of imatinib (STI571) in metastatic gastrointestinal stromal tumours: a phase I study. Lancet 2001;358:1421–3.
8. Heinrich MC, Corless CL, Blanke CD, et al. Molecular correlates of imatinib resistance in gastrointestinal stromal tumors. J Clin Oncol 2006;24:4764–74.
9. Debiec-Rychter M, Sciot R, Le Cesne A, et al. KIT mutations and dose selection for imatinib in patients with advanced gastrointestinal stromal tumours. Eur J Cancer 2006;42:1093–103.
10. Debiec-Rychter M, Dumez H, Judson I, et al. Use of c-KIT/PDGFRA mutational analysis to predict the clinical response to imatinib in patients with advanced gastrointestinal stromal tumours entered on phase I and II studies of the EORTC Soft Tissue and Bone Sarcoma Group. Eur J Cancer 2004;40:689–95.
11. Schneider-Stock R, Boltze C, Lasota J, et al. Loss of p16 protein defines high-risk patients with gastrointestinal stromal tumors: a tissue microarray study. Clin Cancer Res 2005;11:638–45.
12. Schneider-Stock R, Boltze C, Lasota J, et al. High prognostic value of p16INK4 alterations in gastrointestinal stromal tumors. J Clin Oncol 2003;21:1688–97.
13. Rumessen JJ, Peters S, Thuneberg L. Light- and electron microscopical studies of interstitial cells of Cajal and muscle cells at the submucosal border of human colon. Lab Invest 1993;68:481–95.
14. Tornillo L, Duchini G, Carafa V, et al. Patterns of gene amplification in gastrointestinal stromal tumors (GIST). Lab Invest 2005;85:921–31.
15. El-Rifai W, Sarlomo-Rikala M, Andersson LC, Knuutila S, Miettinen M. DNA sequence copy number changes in gastrointestinal stromal tumors: tumor progression and prognostic significance. Cancer Res 2000;60:3899–903.
16. Kang HJ, Nam SW, Kim H, et al. Correlation of KIT and platelet-derived growth factor receptor α mutations with gene activation and expression profiles in gastrointestinal stromal tumors. Oncogene 2005;24:1066–74.
17. Koon N, Schneider-Stock R, Sarlomo-Rikala M, et al. Molecular targets for tumour progression in gastrointestinal stromal tumours. Gut 2004;53:235–40.
18. Antonescu CR, Viale A, Sarran L, et al. Gene expression in gastrointestinal stromal tumors is distinguished by KIT genotype and anatomic site. Clin Cancer Res 2004;10:3282–90.
19. Petricoin EF, Ardekani AM, Hitt BA, et al. Use of proteomic patterns in serum to identify ovarian cancer. Lancet 2002;359:572–7.
20. Suehara Y, Kondo T, Fujii K, et al. Proteomic signatures corresponding to histological classification and grading of soft-tissue sarcomas. Proteomics 2006;6:4402–9.
21. Chen G, Gharib TG, Wang H, et al. Protein profiles associated with survival in lung adenocarcinoma. Proc Natl Acad Sci U S A 2003;100:13537–42.
22. Okano T, Kondo T, Fujii K, et al. Proteomic signature corresponding to the response to gefitinib (Iressa, ZD1839), an epidermal growth factor receptor (EGFR) tyrosine kinase inhibitor, and mutation in EGFR in lung adenocarcinoma. Clin Cancer Res 2007;13:799–805.
23. Orntoft TF, Thykjaer T, Waldman FM, Wolf H, Celis JE. Genome-wide study of gene copy numbers, transcripts, and protein levels in pairs of non-invasive and invasive human transitional cell carcinomas. Mol Cell Proteomics 2002;1:37–45.
24. Varambally S, Yu J, Laxman B, et al. Integrative genomic and proteomic analysis of prostate cancer reveals signatures of metastatic progression. Cancer Cell 2005;8:393–406.
25. Resendes BL, Kuo SF, Robertson NG, et al. Isolation from cochlea of a novel human intronless gene with predominant fetal expression. J Assoc Res Otolaryngol 2004;5:185–202.
26. Stankey RH LA. Pathology and Genetics of Tumours of the Digestive System. Lyon: IARC Press; 2000.
27. Hasegawa T, Matsuno Y, Shimoda T, Hirohashi S. Gastrointestinal stromal tumor: consistent CD117 immunostaining for diagnosis, and prognostic classification based on tumor size and MIB-1 grade. Hum Pathol 2002;33:669–76.
28. Unlu M, Morgan ME, Minden JS. Difference gel electrophoresis: a single gel method for detecting changes in protein extracts. Electrophoresis 1997;18:2071–7.
29. Yokoo H, Kondo T, Fujii K, Yamada T, Todo S, Hirohashi S. Proteomic signature corresponding to α fetoprotein expression in liver cancer cells. Hepatology 2004;40:609–17.
30. Okano T, Kondo T, Kakisaka T, et al. Plasma proteomics of lung cancer by a linkage of multi-dimensional liquid chromatography and two-dimensional difference gel electrophoresis (2D-DIGE). Proteomics 2006;6:3938–48.
31. Yoshida Y, Shibata T, Kokubu A, et al. Mutations of the epidermal growth factor receptor gene in atypical adenomatous hyperplasia and bronchioloalveolar carcinoma of the lung. Lung Cancer 2005;50:1–8.
32. Kaplan EL, Meier P. Nonparametric estimation from incomplete observations. J Am Stat Assoc 1958;53:457–81.
33. Kang HJ, Koh KH, Yang E, et al. Differentially expressed proteins in gastrointestinal stromal tumors with KIT and PDGFRA mutations. Proteomics 2006;6:1151–7.
34. Molina H, Horn DM, Tang N, Mathivanan S, Pandey A. Global proteomic profiling of phosphopeptides using electron transfer dissociation tandem mass spectrometry. Proc Natl Acad Sci U S A 2007;104:2199–204.
35. Matsuoka S, Ballif BA, Smogorzewska A, et al. ATM and ATR substrate analysis reveals extensive protein networks responsive to DNA damage. Science 2007;316:1160–6.
36. Lasota J, Jasinski M, Sarlomo-Rikala M, Miettinen M. Mutations in exon 11 of c-Kit occur preferentially in malignant versus benign gastrointestinal stromal tumors and do not occur in leiomyomas or leiomyosarcomas. Am J Pathol 1999;154:53–60.
37. Ernst SI, Hubbs AE, Przygodzki RM, Emory TS, Sobin LH, O'Leary TJ. KIT mutation portends poor

prognosis in gastrointestinal stromal/smooth muscle tumors. Lab Invest 1998;78:1633–6.

38. Hirota S, Isozaki K, Nishida T, Kitamura Y. Effects of loss-of-function and gain-of-function mutations of c-kit on the gastrointestinal tract. J Gastroenterol 2000; 35 Suppl 12:75–9.

39. Wardelmann E, Losen I, Hans V, et al. Deletion of Trp-557 and Lys-558 in the juxtamembrane domain of the c-kit protooncogene is associated with metastatic behavior of gastrointestinal stromal tumors. Int J Cancer 2003;106:887–95.

40. Lasota J, Dansonka-Mieszkowska A, Stachura T, et al. Gastrointestinal stromal tumors with internal tandem duplications in 3′ end of KIT juxtamembrane domain occur predominantly in stomach and generally seem to have a favorable course. Mod Pathol 2003; 16:1257–64.

41. Antonescu CR, Sommer G, Sarran L, et al. Association of KIT exon 9 mutations with nongastric primary site and aggressive behavior: KIT mutation analysis and clinical correlates of 120 gastrointestinal stromal tumors. Clin Cancer Res 2003;9: 3329–37.

42. Montgomery E, Abraham SC, Fisher C, et al. CD44 loss in gastric stromal tumors as a prognostic marker. Am J Surg Pathol 2004;28:168–77.

43. Nishitani A, Hirota S, Nishida T, et al. Differential expression of connexin 43 in gastrointestinal stromal tumours of gastric and small intestinal origin. J Pathol 2005;206:377–82.

44. Klose J, Nock C, Herrmann M, et al. Genetic analysis of the mouse brain proteome. Nat Genet 2002;30: 385–93.

45. Kondo T, Hirohashi S. Application of highly sensitive fluorescent dyes (CyDye DIGE Fluor saturation dyes) to laser microdissection and two-dimensional difference gel electrophoresis (2D-DIGE) for cancer proteomics. Nat Protoc 2006;1: 2940–56.

Bone Marrow Transplantation (2008) 41, 1067–1068

www.nature.com/bmt

LETTER TO THE EDITOR

Segregated graft-versus-tumor effect between CNS and non-CNS lesions of Ewing's sarcoma family of tumors

Bone Marrow Transplantation (2008) **41,** 1067–1068; doi:10.1038/bmt.2008.26; published online 10 March 2008

For patients with the localized Ewing's sarcoma family of tumors (ESFT), first-line multimodal treatment, including intensive multi-agent chemotherapy, local radiation therapy and surgery, produces 70–75% of the long-term survival rate.[1,2] However, once patients relapse, there is no effective treatment that yields a 5-year survival rate exceeding 20%, even with high-dose chemotherapy (HDC) with autologous stem cell rescue.[3,4] Therefore, a new and more effective treatment approach is clearly needed for this population. Several reports have described patients with ESFT who had bone marrow metastases and underwent allogeneic SCT instead of autologous SCT,[5] including a rare patient who exhibited evidence of a graft-versus-tumor (GVT) effect.[6] To accumulate further knowledge, we report the case of a patient with recurrent ESFT who responded to allogeneic SCT from a sibling donor. A unique aspect of this case was that the manifestation of the GVT effect differed in different organs, with involvement of central nervous system (CNS) and non-CNS lesions. The GVT effect is rare in CNS diseases.

A 28-year-old woman was diagnosed with ESFT of the right chest wall. The tumor size was $10 \times 11 \times 8$ cm and no metastases were shown on computed tomography (CT) or bone scans. Histology revealed small, round cells positive for the cell-surface glycoprotein CD99 and negative for desmin, myoD1, S100 protein, CD45 and CD30. Primary treatment comprised of two courses of chemotherapy with vincristine, doxorubicin and cyclophosphamide (VDC), followed by two courses of ifosfamide, and then HDC with thiotepa 300 mg/m^2 for 2 days and etoposide 300 mg/m^2 for 3 days with autologous peripheral blood stem cell rescue. Local radiation therapy with 50 Gy X-ray was also administered. The patient remained well without evidence of recurrent disease until 20 months after the autologous SCT, when she presented with chest pain and a recurrent tumor in the original site was observed on CT scanning (Figure 1a). After four courses of re-induction chemotherapy, including one course of VDC, one course of ifosfamide and etoposide (IE), and two courses of irinotecan, and HDC consisting of etoposide 200 mg/m^2 for 4 days and melphalan 90 mg/m^2 for 2 days with autologous peripheral blood stem cell rescue, she achieved partial remission (Figure 1b). The patient then entered a phase I/II clinical trial of reduced-intensity allogeneic SCT. After

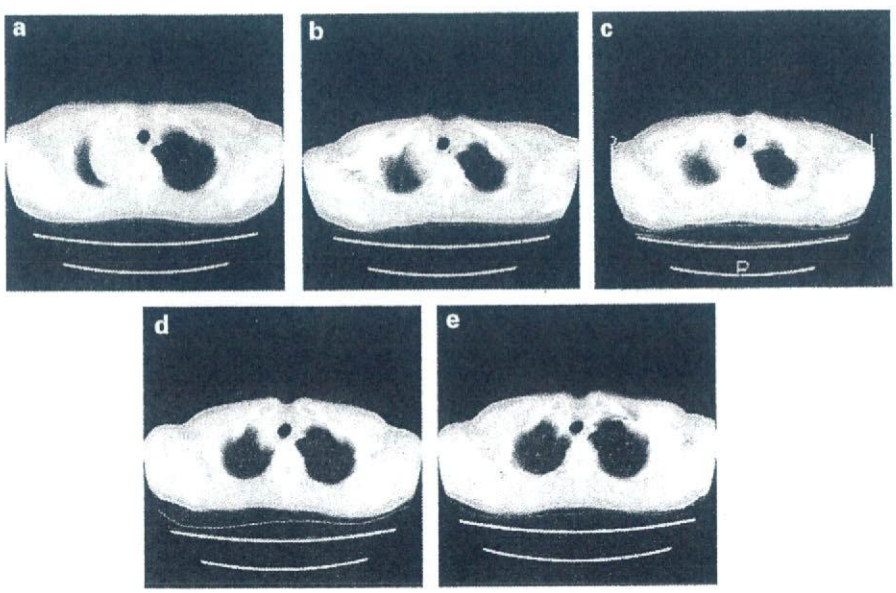

Figure 1 (**a**) Computed tomography (CT) images of a primitive neuroectodermal tumor in the apical lesion on relapse after autoperipheral blood SCT. (**b**) After four courses of chemotherapy, the patient achieved partial remission. A CT scan taken 1 month after the allogeneic SCT, the tumor size was almost no change (**c**), but 4 months after, it showed 50% reduction of the apical tumor (**d**). CR was confirmed at 8 months (**e**).

preconditioning with busulfan (4 mg/kg/day, orally from day −4 to day −3) and fludarabine (30 mg/m^2/day, intravenously from day −8 to day −3), peripheral blood cells containing 2.4×10^6/kg CD34$^+$ cells from her HLA-matched sister were infused. Prophylactic immunosuppression with cyclosporine-A was started on day −1. Her post transplant course was uncomplicated, except for transient grade 1 GVHD of the skin, which began on day +64 and resolved by day +67 without any specific treatment. Cyclosporine-A was tapered from day +70 and discontinued on day +106. A CT scan taken 1 month after the allogeneic SCT when the tumor size was almost unchanged (Figure 1c), but 4 months later, there was 50% reduction of the apical tumor (Figure 1d). CR was confirmed at 8 months (Figure 1e). The patient had headache and was found to have CNS disease on magnetic resonance imaging at 14 months. She died of the disease 5 months after the second relapse. The patient relapsed after initial treatment including HDC with autologous stem cell support, but thereafter, the tumor disappeared coincidently with the occurrence of GVHD, and at least for the primary lesion, the regression period exceeded the period of initial remission. Hence, a graft-versus-ESFT effect seems likely.

In this case, we followed the patient mainly by CT scanning. Although the CT findings showed the tumor status fairly well, they could not provide information regarding viability of the residual tumor. In this regard, PET scanning would be very helpful.

Interestingly, although the GVT effect was exerted in the primary lesion in the chest wall, it was not effective for the prevention of CNS recurrence in this case. The speculated reason for this observation is that the CNS is essentially an immunologically privileged site and theoretically, donor-derived immunocompetent cells carrying the GVT effect mechanism cannot cross the blood–brain barrier.[7] Hence, the application of additional therapeutic intervention to the CNS might become necessary after any systemic manifestations of a GVT effect.

A Hosono[1], A Makimoto[1], A Kawai[2] and Y Takaue[3]
[1]*Division of Pediatric Oncology, National Cancer Center Hospital, Tokyo, Japan;*
[2]*Division of Orthopedic Surgery, National Cancer Center Hospital, Tokyo, Japan and*
[3]*Division of Hematopoietic Stem Cell Transplantation, National Cancer Center Hospital, Tokyo, Japan*
E-mail: ahosono@ncc.go.jp

References

1 Marina NM, Pappo AS, Parham DM, Cain AM, Rao BN, Poquette CA *et al.* Chemotherapy dose-intensification for pediatric patients with Ewing's family of tumors and desmoplastic small round cell tumor: a feasibility study at St Jude Children's Research Hospital. *J Clin Oncol* 1999; **17**: 180–190.
2 Grier HE, Krailo MD, Tarbell NJ, Link MP, Fryer CJ, Pritchard DJ *et al.* Addition of ifosfamide and etoposide to standard chemotherapy for Ewing's sarcoma and primitive neuroectodermal tumor of bone. *N Engl J Med* 2003; **348**: 694–701.
3 Barker LM, Pendergrass TW, Sanders JE, Hawkins DS. Survival after recurrence of Ewing's sarcoma family of tumors. *J Clin Oncol* 2005; **23**: 4354–4362.
4 Galindo CR, Billups CA, Kun LE, Rao BN, Pratt CB, Merchant TE *et al.* Survival after recurrence of Ewing tumors. *Cancer* 2002; **94**: 561–569.
5 Burdach S, Kaick BV, Laws HJ, Ahrens S, Haase R, Korholz D *et al.* Allogenic and autologous stem-cell transplantation in advanced Ewing tumors. *Ann Oncol* 2000; **11**: 1451–1462.
6 Koscielniak E, Wieltsch U, Treuner J, Winker P. Graft-versus-Ewing sarcoma effect and long-term remission induced by haploidentical stem-cell transplantation in a patient with relapse of metastatic disease. *J Clin Oncol* 2005; **23**: 242–248.
7 Carson CM, Sutcliffe JG. Balancing function vs. self-defense: the CNS as an active regulator of immune response. *J Neurosci Res* 1999; **55**: 1–8.

Clin Orthop Relat Res (2008) 466:2099–2106
DOI 10.1007/s11999-008-0330-4

SYMPOSIUM: MOLECULAR GENETICS IN SARCOMA

Global Protein-expression Analysis of Bone and Soft Tissue Sarcomas

Akira Kawai MD, PhD, Tadashi Kondo MD, PhD, Yoshiyuki Suehara MD, PhD, Kazutaka Kikuta MD, Setsuo Hirohashi MD, PhD

Published online: 6 June 2008

Abstract Analysis of global protein expression, an approach known as expression proteomics, can offer important clues for understanding tumor biology that cannot be obtained by other approaches (e.g., genome or transcriptome analysis). Using two-dimensional difference gel electrophoresis (2D-DIGE) and mass spectrometry, we performed global protein expression studies of bone and soft tissue sarcomas to develop novel diagnostic and therapeutic biomarkers and allow molecular classification of the tumors. Among 1500 protein variants identified in the two-dimensional gel, 67 proteins correctly distinguished the eight subtypes of 99 histologically classified soft tissue sarcomas. Hierarchical clustering demonstrated leiomyosarcoma and MFH shared a similar protein expression profile, and clear cell sarcoma, synovial sarcoma, and MPNST could be grouped according to their protein expression patterns. Pleomorphic leiomyosarcoma and MFH showed similar tropomyosin isoform expression patterns. Patients with gastrointestinal stromal tumors expressing pfetin protein had better survival than those whose tumors lacked it. We identified 10 protein spots associated with the chemosensitivity of osteosarcoma to preoperative chemotherapy. These 10 spots could be new diagnostic and prognostic markers for osteosarcoma and new therapeutic targets for the disease. Proteomic analysis using 2D-DIGE provides novel information on the biology of bone and soft tissue sarcomas that could be used to diagnosis and treat these tumors.
Level of Evidence: Level II, diagnostic study. See the Guidelines for Authors for a complete description of levels of evidence.

This work was supported by a grant from the Ministry of Health, Labor and Welfare (AK, TK), a grant from the Ministry of Education, Science, Sports, and Culture (AK), and a grant from the Program for Promotion of Fundamental Studies in Health Sciences of the National Institute of Biomedical Innovation of Japan (TK).
Each author certifies that his or her institution has approved the human protocol for this investigation and that all investigations were conducted in conformity with ethical principles of research.

A. Kawai (✉), Y. Suehara, K. Kikuta
Division of Orthopaedic Surgery, National Cancer Center Hospital, 5-1-1 Tsukiji, Chuo-ku, Tokyo, Japan
e-mail: akawai@ncc.go.jp

T. Kondo, S. Hirohashi
Proteome Bioinformatics Project, National Cancer Center Research Institute, Tokyo, Japan

Y. Suehara
Department of Orthopaedic Surgery, Juntendo University School of Medicine, Tokyo, Japan

Introduction

Over the past three decades, advances in diagnostic modalities and treatment methods have substantially improved the survival rate and postoperative limb function of patients with bone and soft tissue sarcomas [5, 10, 20, 27, 40]. Wide excision of tumors in conjunction with multiagent chemotherapy now provides 5-year disease-specific survivals ranging from 60% to 80% in patients with localized high-grade sarcomas [2, 5, 27]. Despite this success, the outcomes of patients who have metastatic disease at diagnosis or those with tumors showing a poor response to chemotherapy are still unsatisfactory (5-year disease-specific survival rates, 20%–40%), even with dose-intensive or high-dose chemotherapy [9, 18, 19, 33]. For improving the prognosis of patients with these difficult-to-treat sarcomas, it is imperative to develop new targeted therapeutic strategies based on an understanding of the

biologic mechanisms underlying the metastasis and chemoresistance of these tumors.

Recent development of high-throughput screening techniques has allowed global investigations of the molecular backgrounds associated with the clinicopathologic characteristics of tumors. A DNA microarray-based approach allows the screening of several thousand mRNAs in bone and soft tissue sarcomas and can identify the genes relevant to their histologic diagnosis, clinical features, and chemosensitivity [39]. Using an oligonucleotide microarray approach, Nakayama et al. [31] analyzed gene expression in 105 soft tissue sarcoma samples and reclassified malignant fibrous histiocytoma (MFH), which has a wide variety of clinicopathologic features, into pleomorphic subtypes of other distinct types of sarcomas. Based on gene-expression profiles, Ochi et al. [34] identified 60 genes whose expression levels were likely correlated with the chemosensitivity of osteosarcomas. Mintz et al. [29] reported 104 genes were differentially expressed between chemotherapy-sensitive and -resistant osteosarcomas.

Although much evidence suggests genetic abnormalities play a primary role in the development of tumors, there is also evidence for the effects of aberrations that cannot be detected solely by genome (DNA sequencing) or transcriptome (measurement of all mRNA in a population of cells) analysis: posttranslational modifications of proteins such as phosphorylation, glycosylation, and degradation, are aberrantly regulated in many types of cancers and cannot be predicted by DNA sequencing or measurement of mRNA expression. It has become evident there is considerable discrepancy between expression of mRNA and that of protein [4, 12]. Further, proteins are more directly linked to aberrant tumor phenotypes. These difficulties underline the potential advantages of monitoring protein expression in a global manner, an approach known as expression proteomics. In addition, the results obtained from proteomic studies will be more easily applicable to the clinical field with the use of specific antibodies.

We have performed global protein expression studies using our original high-throughput two-dimensional difference gel electrophoresis (2D-DIGE) system on several types of tumors [21, 22]. This approach has proven useful for classifying soft tissue sarcomas at the protein expression level and for identifying novel diagnostic and prognostic markers [37]. Biomarkers specifically expressed in a specific subgroup of tumors can facilitate a risk-adopted tailored medical treatment. Examination of the markers may allow the identification of a high-risk patient group that may benefit from adjuvant therapy, whereas it may also help spare low-risk patients unnecessary treatment. Moreover, specifically expressed molecules or associated pathways could be crucial molecular targets to allow for more selective therapeutic intervention.

We report our approach for identifying biomarkers that associate with clinicopathologic features of bone and soft tissue sarcomas using global protein expression analysis.

Materials and Methods

We performed protein expression profiling for 99 soft tissue sarcomas: 28 MFHs, 19 rhabdomyosarcomas, 12 synovial sarcomas, 10 leiomyosarcomas, 10 myxoid liposarcomas, nine gastrointestinal stromal tumors (GIST), six clear cell sarcomas, and five malignant peripheral nerve sheath tumors (MPNST) using 2D-DIGE. We used the term "MFH" to describe tumors diagnosed as storiform and pleomorphic-type MFH that showed predominant pleomorphic features without any findings of a specific type of differentiation. All tumor samples were obtained from patients treated at the National Cancer Center Hospital (Tokyo, Japan). We snap-froze fresh-frozen samples in liquid nitrogen immediately after resection or biopsy sampling before any treatment and stored them at −80°C until use. Tumor samples for immunohistochemical analysis were preserved in archival paraffin-embedded tissue blocks. This study was approved by the Institutional Review Board and conducted according to tenets of the Declaration of Helsinki.

Protein expression profiles were studied by 2D-DIGE as described previously [21, 22]. For protein extraction, the frozen samples were homogenized with urea lysis buffer (6 M urea, 2 M thiourea, 3% CHAPS, 1% Triton X-100). After centrifugation at 15,000 rpm for 30 minutes, the supernatant was used for studies. A mixture of all the experimental samples was used as an internal control sample. The internal control and individual samples were labeled with fluorescent dyes with different excitation and emission wavelengths (CyDye DIGE Fluor saturation dye; Amersham Biosciences, Little Chalfont, Buckinghamshire, UK): Cy3 for the internal control and Cy5 for the individual samples. The Cy3-labeled control sample and the Cy5-labeled individual sample were mixed and coseparated by two-dimensional polyacrylamide gel electrophoresis. The first-dimensional separation was performed using an immobilized pH gradient gel (length 24 cm, p*I* range 3-10; Amersham Biosciences) in accordance with the manufacturer's recommended protocol. The immobilized pH gradient gels were then equilibrated and transferred to 9% to 16% polyacrylamide gradient gels measuring 24 cm × 20 cm. The gels were run in an Ettan Dalt II system (Amersham Biosciences) at 18 W and 18°C for 15 hours. Each sample was run on triplicate gels and the average spot intensities were calculated for quantitative analysis.

After electrophoresis, the gels were scanned at appropriate wavelengths for Cy3 and Cy5 using a 2-D 2920

MasterImager (Amersham Biosciences) [21, 22]. The ratio of Cy5 intensity to Cy3 intensity was calculated for all spots in each gel with DeCyder software (Amersham Biosciences) to obtain the standardized spot intensities. Because the Cy3 image represents the internal standard sample, this standardization procedure eliminates gel-to-gel differences. Approximately 1500 protein spots were visualized by laser scanning (Fig. 1). The standardized spot intensities were logarithmically transformed and analyzed with the data-mining package Impressionist (GeneData, Basel, Switzerland).

We identified informative proteins using a support vector machine algorithm with leave-one-out crossvalidation. The classification performance of a candidate classifier was evaluated by multivariate analysis, including principal component analysis and hierarchical clustering. Proteins corresponding to the spots of interest were identified by mass spectrometric analysis using a matrix laser desorption/absorption/ionization (MALDI) time of flight mass spectrometer. Protein identification and differential expression were confirmed by Western blotting using specific antibodies.

Immunohistochemical analysis was performed according to the streptavidin-biotin peroxidase method using a Strept ABC Complex/HRP kit (DAKO, Tokyo, Japan) on formalin-fixed paraffin-embedded tissues. Rabbit polyclonal antibody against pfetin was kindly provided by Dr Morton [35]. Two reviewers (YS, AK) reviewed the results of immunohistochemical staining in a blinded fashion regarding the clinical data.

We calculated tumor-specific survival time from the first resection of primary tumor to death from tumor-specific causes. Patients who died of causes unrelated to the disease were censored at the time of death. All time to event end points were computed using the Kaplan and Meier method. We used the log-rank test to determine differences in survival between subgroups. We used the Cox proportional hazards regression to analysis differences in survival after adjusting for potentially confounding variables (site, size, differentiation and pfetin).

To identify markers associated with osteosarcoma chemosensitivity, we analyzed the protein expression profiles of 23 biopsy samples of typical osteosarcoma (conventional central high-grade osteosarcomas that had developed in long tubular bones in patients with a mean age of 18 years). All the patients received standard pre- and postoperative chemotherapy consisting of high-dose methotrexate, cisplatin, doxorubicin, and ifosfamide. The histologic effects of preoperative chemotherapy according to the Huvos grading system [36] were Grade I in seven cases, Grade II in seven, Grade III in six, and Grade IV in three. We compared the protein expression profiles of two distinct groups; nine samples from patients showing a good response to preoperative chemotherapy (greater than 90% tumor necrosis; Huvos Grades III and IV) and seven samples from patients showing a poor response (less than 50% tumor necrosis; Huvos Grade I).

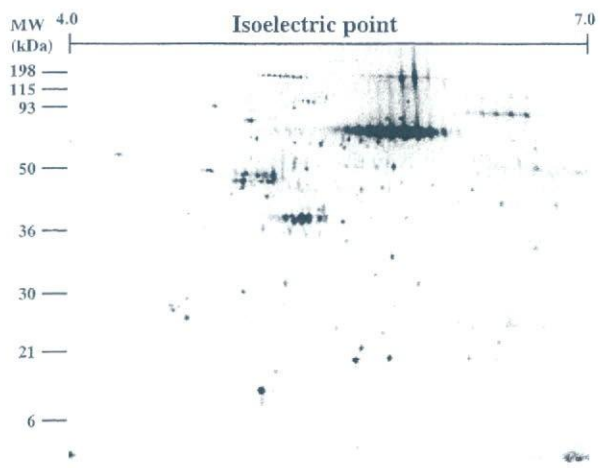

Fig. 1 Representative two-dimensional image of Cy5-labeled proteins of osteosarcoma. Approximately 1500 protein spots are visualized by laser scanning. Proteins corresponding to the spots of interest were picked up and identified by mass spectrometric analysis.

Results

Hierarchical clustering using all 1500 protein spots did not classify the tumors exactly in accordance with the histologic classification. To examine the possible differences in protein expression between different types of sarcoma, we selected 67 proteins whose expression was associated with the existing histologic classification by using a support vector machine algorithm (Fig. 2). All the tumors were separable into six clusters. Myxoid liposarcomas and rhabdomyosarcomas formed tight clusters on two distinct dendrogram branches. The third and fourth clusters mostly comprised a mixture of leiomyosarcomas and MFHs. The third cluster contained a large proportion of leiomyosarcomas, whereas the fourth cluster contained mostly MFHs together with two cases of pleomorphic leiomyosarcoma and a case of CCS. GISTs formed a distinct fifth cluster. The sixth cluster comprised three different types of sarcomas (CCS, synovial sarcoma, and MPNST) and three outlier cases.

Using supervised analysis of pleomorphic and conventional leiomyosarcomas, we found tropomyosin isoforms were responsible for leiomyosarcoma subtypes. Conventional leiomyosarcoma expressed mainly tropomyosin isoforms 1 and 2, whereas pleomorphic leiomyosarcoma largely expressed tropomyosin isoforms 3 and 4 (Fig. 3). MFH shared an expression pattern of tropomyosin isoforms

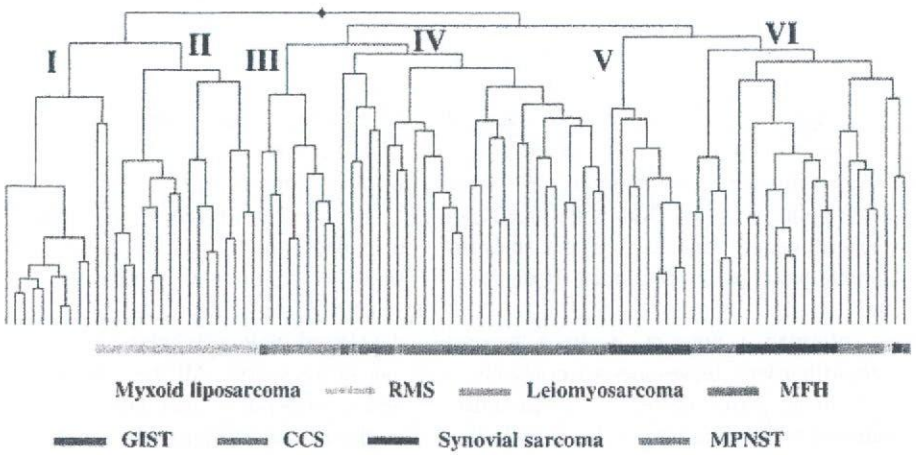

Fig. 2 Hierarchical classification of the 99 soft tissue sarcomas using the selected 67 proteins. The dendrogram shows the degree of similarity of protein expression pattern between the tumors. The shorter the branches, the more similar the two joined tumors. Most tumors formed tight clusters corresponding to their histology except leiomyosarcoma and malignant fibrous histiocytoma. RMS = rhabdomyosarcoma; MFH = malignant fibrous histiocytoma; GIST = gastrointestinal stromal tumor; MPNST = malignant peripheral nerve sheath tumor.

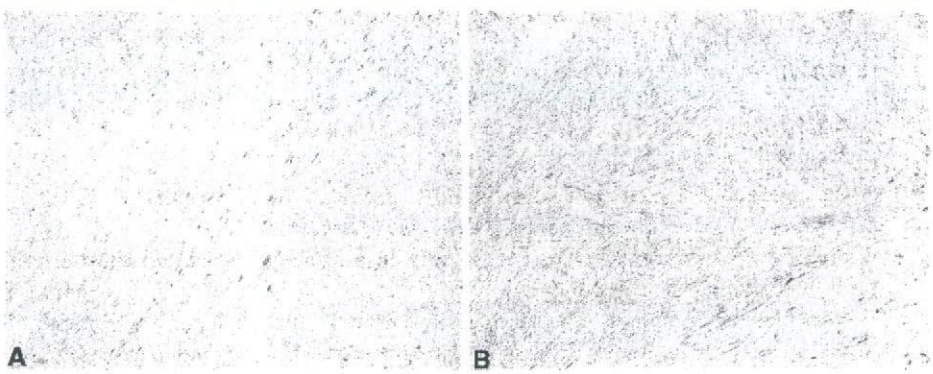

Fig. 3A–B Immunohistochemical staining of tropomyosin isoform type 4. Representative photomicrographs of (**A**) conventional leiomyosarcoma and (**B**) pleomorphic leiomyosarcoma. Tropomyosin isoform 4 is highly expressed in pleomorphic leiomyosarcoma, but not in conventional leiomyosarcoma (stain, immunohistochemical staining for tropomyosin isoform 4; original magnification, ×200).

(mainly types 3 and 4) similar to that of pleomorphic leiomyosarcoma.

By comparing the protein expression profiles of two distinct groups of GISTs—pathologically high-risk and clinically aggressive cases and pathologically low- or intermediate-risk and clinically indolent cases—we identified 43 protein spots whose expression differed (Wilcoxon test, $p < 0.001$) between the two groups. Mass spectrometric identification demonstrated the 43 spots corresponded to 25 distinct gene products, eight of which were derived from a potassium channel protein, pfetin. Western blotting and real-time PCR suggested pfetin expression inversely correlated ($p < 0.0001$) with the development of metastasis. Immunohistochemical analysis revealed patients with tumors expressing pfetin protein had better ($p < 0.0001$) tumor-specific survival than those with tumors lacking pfetin expression (Fig. 4).

By comparing the protein expression profiles (1465 protein spots) of two distinct groups of osteosarcoma biopsy samples—a chemosensitive group (good responders; Huvos

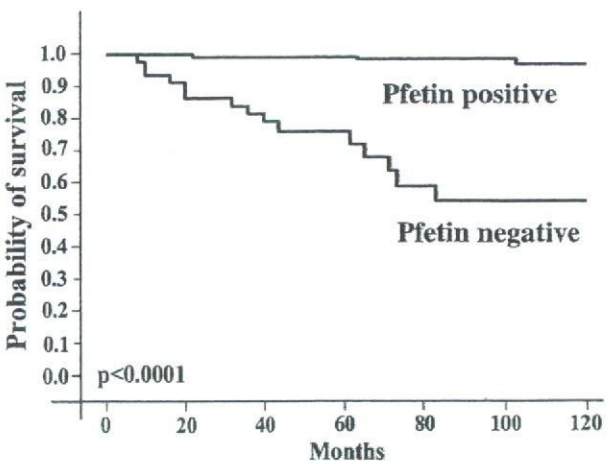

Fig. 4 Tumor-specific survival of 210 patients with M0 gastrointestinal stromal tumors according to the expression of pfetin protein in the primary tumor samples examined by immunohistochemistry. Patients with tumors expressing pfetin ($n = 171$) had better ($p < 0.0001$) survival (5-year survival, 97.2%) than those with tumors lacking pfetin expression ($n = 39$) (5-year survival, 76.5%).

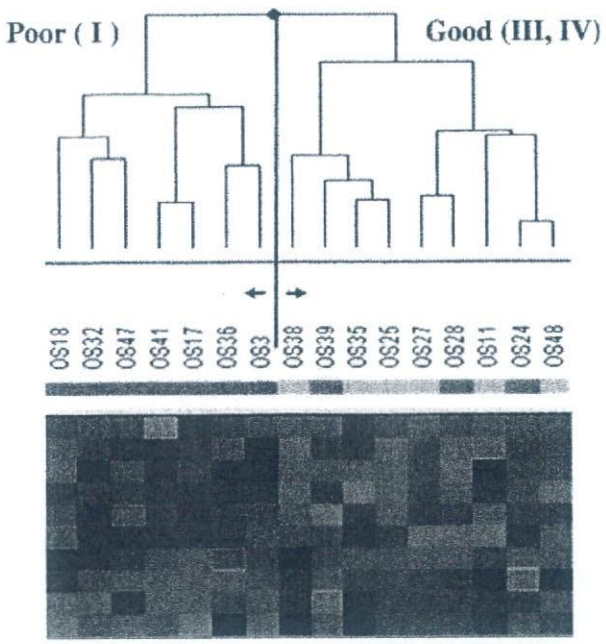

Fig. 5 Expression pattern of the 10 protein spots that discriminate good responders (Huvos Grades III, IV) from poor responders (Huvos Grade I) among 16 patients with osteosarcoma. Horizontal rows represent individual protein spots, and vertical columns represent individual samples. Each cell in the matrix represents the expression level of a single protein spot in a single sample. Red indicates overexpression relative to the expression of the control sample, whereas green indicates underexpression. There are seven spots that are overexpressed in poor responders and three spots overexpressed in good responders.

Grades III and IV) versus a chemoresistant group (poor responders; Huvos Grade I)—we identified 10 protein spots whose expression differed (Wilcoxon test, $p < 0.05$) between the two groups (Fig. 5). Among these 10 spots, the expression levels of seven spots were higher and those of three spots were lower in poor responders compared with good responders. Principal component analysis accurately divided the osteosarcoma samples into good responder and poor responder groups based on the expression levels of the 10 selected classifiers (Fig. 6).

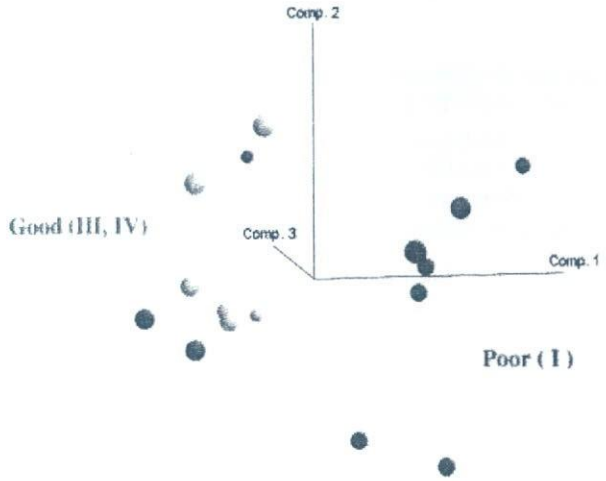

Fig. 6 Principal component analysis of the 16 osteosarcomas on the basis of the expression profiles of the 10 selected protein spots. It accurately classifies the osteosarcoma samples into either good responders (Huvos Grades III, IV) or poor responders (Huvos Grade I).

Discussion

Many lines of evidence have revealed genetic alterations such as activation of oncogenes, inactivation of tumor suppressor genes, and chromosomal translocations play a primary role in the development of bone and soft tissue sarcomas [6, 16, 24]. These genetic alterations initiate changes in a series of signal transduction pathways and develop malignant tumor cells. Although the initial changes occur at the DNA level, all the effects are ultimately expressed as the changes of the protein content. Proteins are considered the hallmark of genetic alterations. Global mRNA expression studies are often performed to follow these changes [29, 30–34]. However, recent comparative studies of mRNA and protein expression in tumor cells revealed only a subset of mRNA correlated with protein abundance [4, 12]. Moreover, posttranslational modifications, which play important roles in tumor biology, cannot be predicted only by mRNA examinations. These limitations of mRNA expression studies underline the potential advantages of monitoring protein expression in a global manner, an approach known as expression proteomics. Recently, using MALDI MS tissue profiling, Holt et al. [14] reported protein peaks that were differentially expressed in high-grade and low-grade soft tissue sarcomas. Among several proteomic technologies, 2D-DIGE has advantages that make it possible to examine hundreds of proteins simultaneously estimating their expression and posttranslational modifications quantitatively [21, 22]. Applications of sensitive fluorescent dyes and laser scanning made it possible to execute large-scale proteomics in a more efficient, accurate, and reproducible way. In the present study, we examined the protein expression profiles of a diverse group of bone and soft tissue sarcomas in relation to their clinicopathologic features using the 2D-DIGE technique.

A limitation of the current 2D-DIGE is the thoroughness of the analysis. Although the method reveals global expression profiles of more than 1000 protein spots quantitatively, it cannot uncover proteins expressed in very low levels. Compared with the cDNA microarray analysis (20,000 probe sets), the sensitivity of the current 2D-DIGE analysis (1500 spots) is unsatisfactory. We are now trying

to improve the sensitivity of 2D-DIGE using a large-format polyacrylamide gel (24 cm × 38 cm) for two-dimensional polyacrylamide gel electrophoresis. Preliminary results demonstrated more protein spots (5000 spots) are quantitatively detected in the large-format two-dimensional gels. We believe such efforts may overcome some of the inherent limitations of the proteomics.

We found 67 proteins correctly distinguished the eight subtypes of 99 soft tissue sarcomas according to their histologic classification. Hierarchical clustering demonstrated leiomyosarcoma and MFH shared a similar protein expression profile, some of which was not distinguishable on the basis of protein expression, and that clear cell sarcoma, synovial sarcoma, and MPNST were grouped according to their protein expression patterns. These results were generally consistent with previous reports based on histologic and transcriptome analyses [7, 13, 19, 25, 30–32].

Using immunohistochemical analysis, Hasegawa et al. [13] demonstrated a large subset of MFH expressed poorly differentiated smooth muscle or myofibroblastic features and should be regarded as pleomorphic leiomyosarcoma or pleomorphic myofibrosarcoma. Fletcher et al. [7] examined 100 cases of so-called MFH histologically and reclassified 20 of the cases as leiomyosarcomas. Considering these findings together with recent DNA microarray and comparative genomic hybridization analyses [25, 31, 32], at least a proportion of MFHs should be reclassified as a pleomorphic subtype of leiomyosarcoma. In this context, pleomorphic leiomyosarcoma and MFH shared similar expression patterns of tropomyosin isoforms.

The similarity of the protein expression profiles of clear cell sarcoma, synovial sarcoma, and MPNST is consistent with the biologic associations and similar gene expression patterns of these tumors. Clear cell sarcoma is also known as melanoma of soft parts and is derived from neural crest progenitor cells [19]. Nagayama et al. [30] reported synovial sarcoma and MPNST shared similar expression patterns of numerous genes related to neural differentiation and suggested synovial sarcoma might be of neuroectodermal origin. On the basis of protein expression patterns, our present results appear to support the assumption that these three tumors are derived from (or differentiate to) neural or neuroectodermal cells.

Currently, the therapeutic strategy for bone and soft tissue sarcomas largely depends on the histologic subtype, grade, and stage of the disease [11, 26]. Although the systems provide valuable information about the clinical behavior of the tumors in most cases, there are several outliers (or patients) in which their clinical course could not be predicted only on the basis of classic appraisals. Moreover, the introduction of molecular-targeted drugs has changed the situation dramatically [8, 28, 41]. Most of these new drugs target a specific molecule, whose presence could not be predicted only from the classic clinicopathologic features. Novel clues for identifying prognostic markers and therapeutic targets in individual tumors are urgently required.

GISTs are the most common mesenchymal tumors of the gastrointestinal tract and are characterized by a wide spectrum of clinical outcomes [41]. Identification of a high-risk group of patients who may benefit from adjuvant therapy such as that including imatinib is an urgent clinical concern. We found 43 proteins, including eight variants of pfetin, which was originally reported as a protein highly expressed in fetal cochlea and brain, were correlated with the outcome of patients with GIST [35, 38]. Although the expression of a whole 43-protein set predicted the outcome of GIST correctly, it seemed difficult to apply the results directly to a hospital setting. Cutting-edge genome or proteome technologies cannot be transferred easily to ordinary clinical examinations. A smaller number of targets, measurable by simpler methods such as immunohistochemistry, is preferable for use in practice. We found expression of pfetin protein, which could be examined immunohistochemically using paraffin-embedded archival tissues, predicted ($p < 0.0001$) disease-specific survival in patients with GIST [38]. Examination of pfetin expression using immunohistochemistry may allow the identification of high-risk patients with GIST who may benefit from adjuvant treatment such as that including imatinib and minimize the risk of unnecessary treatment for low-risk patients.

The prognosis of patients with osteosarcoma has improved markedly as a result of effective chemotherapy. Dose-intensive multiagent chemotherapy continued for 1 year or so has resulted in long-term survival for the majority of patients with localized osteosarcoma [27]. Despite this success, however, 30% to 40% of patients, mainly those with tumors showing a poor response to preoperative chemotherapy, will experience relapse, most often with pulmonary metastases, and die [2]. Prediction of chemosensitivity at the time of diagnosis would therefore be of great clinical importance. Over the last decade, considerable efforts have been made for this purpose. Not only classic parameters such as histologic subtype, tumor location, and presence of metastatic disease at diagnosis [1], but also several molecules related to drug metabolism/transport or tumor development have been reported to correlate with the chemosensitivity of osteosarcoma [3, 15, 17, 23].

Based on the results of cDNA microarray consisting of 23,040 genes, Ochi et al. [34] identified 60 genes whose expression was likely correlated with the chemosensitivity of osteosarcoma and proposed a scoring system based on the expression levels of these genes. Comprehensive analysis of expression levels among thousands of genes enables investigators to identify novel important molecules